Beam Induced Fluorescence Profile Monitor Development at the GSI Report for the Joint Research Activity EU-FP6-CARE-HIPPI.

P. Forck, C. Andre, A. Bank, F. Becker

Gesellschaft für Schwerionenforschung GSI, Darmstadt, Germany

Abstract

Within the HIPPI Joint Research Activity the properties for a non-intercepting beam pro_le measurement are investigated. Due to the high beam power, traditional intercepting methods like SEM-grid or wire scanners might be destroyed. As an alternative method we investigate the monitoring of the _uorescence light emitted by the N2 molecules of the residual gas at blue (molecular ion: 400 to 470 nm) and near UV (neutral molecule 330 to 410 nm). The properties of this _uorescence under various beam conditions at the GSI heavy ion LINAC and synchrotron are carefully investigated. The technical design of such a monitor with modern hardware is described.

Acknowledgements:
We acknowledge the support of the European Community-Research Infrastructure Activity under the FP6 “Structuring the European Research Area” programme (CARE, contract number RII3-CT-2003-506395)

Beam Induced Fluorescence Profile Monitor Development at the GSI – Report for the Joint Research Activity EU-FP6-CARE-HIPPI –

P. Forck, C. Andre, A. Bank, F. Becker
Gesellschaft für Schwerionenforschung GSI, Darmstadt, Germany
e-mail: p.forck@gsi.de

Abstract

Within the HIPPI Joint Research Activity the properties for a non-intercepting beam profile measurement are investigated. Due to the high beam power, traditional intercepting methods like SEM-grid or wire scanners might be destroyed. As an alternative method we investigate the monitoring of the fluorescence light emitted by the N_2 molecules of the residual gas at blue (molecular ion: 400 to 470 nm) and near UV (neutral molecule 330 to 410 nm). The properties of this fluorescence under various beam conditions at the GSI heavy ion LINAC and synchrotron are carefully investigated. The technical design of such a monitor with modern hardware is described.

DEMANDS FOR NON-INTERCEPTING BEAM PROFILE DETERMINATION

The profile of an ion beam can directly be determined by monitoring the fluorescence emitted by the residual gas molecules using a sensitive image intensifier coupled to a CCD camera. This method was previously applied e.g. at cw proton LINACs at Los Alamos [1], CERN PS [2] and SPS synchrotron [3], at ion source energies at Saclay [4] and at COSY [5]. Extensive investigations with beams from the pulsed heavy ion LINAC at GSI and beams extracted from the GSI synchrotron SIS18 are undertaken in the frame of the Joint Research Activity HIPPI and are discussed here. At the LINAC the most important goal is to monitor the profile within one macro pulse of about 200 μs length, e.g. used to fill the proceeding synchrotron. The short beam delivery times disable the possibility for long integration times normally used to improve the signal-to-noise ratio. These investigations are extended for beams of 100 to 1000 MeV/u as extracted from the GSI synchrotron. The main goal here is related to the high currents expected for the planned FAIR facility. Even though most projects within HIPPI have slightly different beam parameters, the design and the achieved results can be adapted for this application. Moreover, the new design uses a digital CCD camera, which fulfills the need of distributed beam diagnostic devices within a large accelerator facility.

The traditional determination of transverse beam profiles by secondary emission grids (SEM-grids) can not be applied at the high current operation at the GSI LINAC with up to 20 mA electrical current for the full macro-pulse length due to the large energy release of the ion beam (maximal 1 MW beam power) in the intercepting material. Not

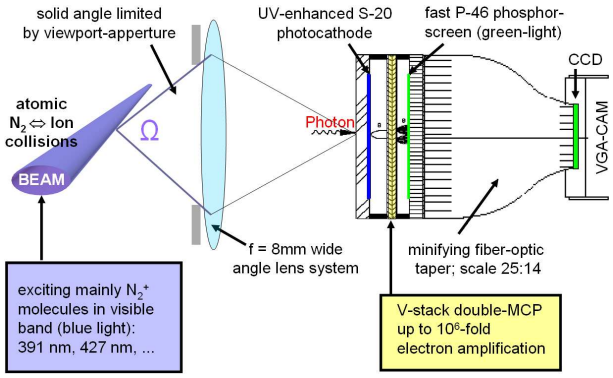

Figure 1: BIF-principle and the scheme of an image intensifier.

to risk melting, the macro-pulse length has to be shorted in case of intercepting diagnostics. For the full pulse length a non-intercepting residual gas monitor can be used or the fluorescence of the residual gas within a so called **B**eam **I**nduced **F**luorescence **BIF** Monitor can be detected. The scheme is shown in Fig. 1 and 2. The BIF Monitor has the advantage that no mechanical parts, and therefore no extra apertures are installed in the vacuum pipe, leading to a compact and cost efficient design. In addition, the spatial resolution for a SEM-grid is limited by the wire spacing of about 1 mm. Using the fluorescence method, up to 0.1 mm can be achieved. Another advantage is the cheap and reliable commercial 'data acquisition system' integrated in the CCD camera.

At the GSI LINAC the ion's kinetic energy varies from 0.12 MeV/u after the first module up to the final LINAC energy of 15 MeV/u. Depending on the ion species and its charge state, this is close to the maximum of the elec-

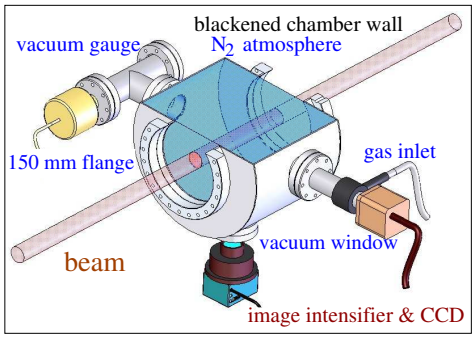

Figure 2: Schematics of a BIF Monitor installation.

tronic stopping power. The residual gas at the LINAC has a typical pressure of 10^{-7} mbar containing mainly Nitrogen.

RELEVANT MOLECULAR PHYSICS

N_2 has a large cross section for the excitation in the neutral and ionized N_2^+ molecular states, as measured in [6] by 200 keV proton collisions and displayed in Fig. 3. Due to the non-resonant excitation process, a scaling proportional to the electronic stopping power of the beam ions is expected. Via optical transitions two bands are emitting in the blue and near UV range, namely the ionized N_2^+ at a band

$$B^2\Sigma_u^+(v') \rightarrow X^2\Sigma_g^+(v'') + \gamma \quad (1)$$

with prominent peaks at 391 nm, 428 nm and 470 nm for the different upper v' and lower v'' vibrational states. The upper electronics state $B^2\Sigma_u^+$ can be accessed by a single step excitation. At slightly shorter wavelength prominent transitions within the neutral N_2 band

$$C^3\Pi_u(v') \rightarrow B^3\Pi_g(v'') + \gamma \quad (2)$$

band is observed with lines between 337 nm and 380 nm. Only by a two step process via collisions with the generated secondary electrons, the upper level is populated due to the necessary spin flip with respect to the neutral $X^1\Sigma_g^+$ ground state. This process might be important for the BIF Monitor, because in a first step the ionizing collisions between the beam ions and N_2 cause free electrons. In the second step these electrons can excite N_2 from the ground state $X^1\Sigma_g^+$ to triplet-states $C^3\Pi_u$ leading to fluorescence-light in the near UV. A quadratic pressure dependence is expected for this process. The lifetime of both upper electronic molecular levels had been determined [7] to be about 60 ns for the ionic and 40 ns for the neutral state. Measurements at GeV proton and ion beams at CERN PS and SPS [2, 3] confirmed the results determined at much lower energies.

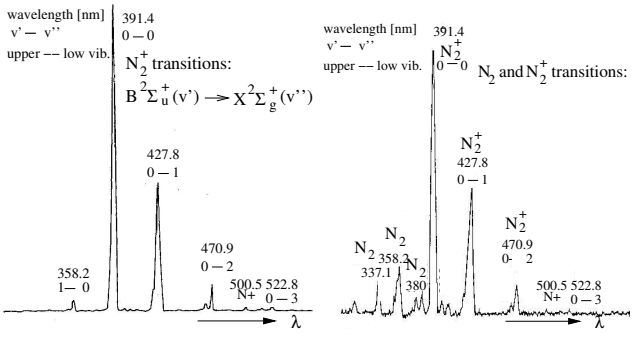

Figure 3: Spectrum from N_2 gas by 200 keV proton impact for lower pressure (left) and high pressure of $\simeq 2 \cdot 10^{-2}$ mbar as determined in the year 1961, see Ref. [6].

TECHNICAL REALIZATION FOR THE BIF MONITOR

First tests are done at a dedicated target location. Now the monitor is mounted behind the GSI Alvarez-section

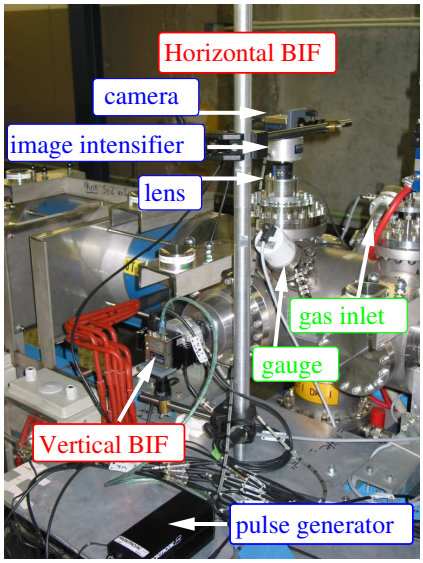

Figure 4: The installation of a horizontal and vertical BIF Monitor at GSI LINAC.

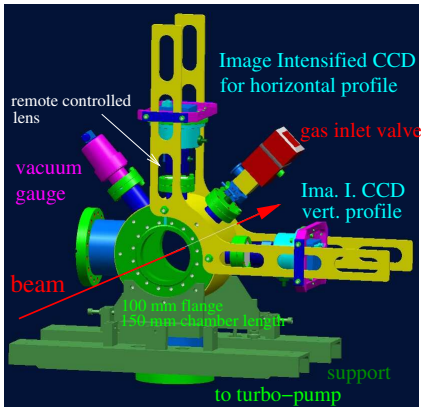

Figure 5: Technical drawing for the vacuum chamber of the BIF Monitor.

having a nominal beam energy of 11.4 MeV/u as depicted in Fig. 4. The emitted fluorescence is detected by an image intensified camera with a total detection efficiency of ~20 % of the photons arriving at the photo-cathode. The main components of the BIF system are described in the following:

Mechanics and vacuum chamber: The photons caused by the interaction of the residual gas and the beam are viewed through a Suprasil (wavelength transmission between 200 nm and 2 μm) window mounted on a Ø 35 mm flange, resulting in a ~5 cm observation length in beam direction. To suppress reflections, the tube is blackened by vacuum suitable graphite lacquer (graphite grains solved in isopropanol). A compact vacuum chamber with only 150 mm insertion length was produced and is shown in Fig. 5.

Regulated gas valve: To increase the gas pressure in the interaction chamber, a regulated gas-inlet has to be used. We use a commercial system from company Pfeiffer, which is remote controlled by the RCV 300 controller via RS232 interface. A maximal pressure of 10^{-4} mbar is tolerable at the LINAC. Behind the synchrotron a pressure up to 1

mbar is allowed, because a 50 μm thick stainless steel vacuum window separates the target location from the transferlines.

Calibration installation: An array of LEDs opposite to the camera is used to match the depth of field with the center of the beam pipe. It also serves as an online calibration for the reproduction scale, i.e. the factor for the conversion from pixel to a mm scale at the beam location.

Lens system: For the first tests, a remote controlled C-mount zoom lens (Fujinon D14$\times$7.5A-R11/12) with $7.5 - 105$ mm focal length and a macro setting was installed having its image plane 390 mm apart from the beam center. A short distance is preferred to capture more photons due to a large solid angle. A small focal length results in a larger depth of field, i.e. with the same relative iris setting a larger depth can be achieved. For the permanent installation a fixed focal length system with remote controlled iris (Pentax C1614ER) is used; this lens is shown in Fig. 6. It has a 16 mm focal length and a distance of 150 mm from the beam axis. The chosen configuration of lens, image intensifier size, taper and CCD camera results in a scaling of about 200 μm/pixel for the beam image.

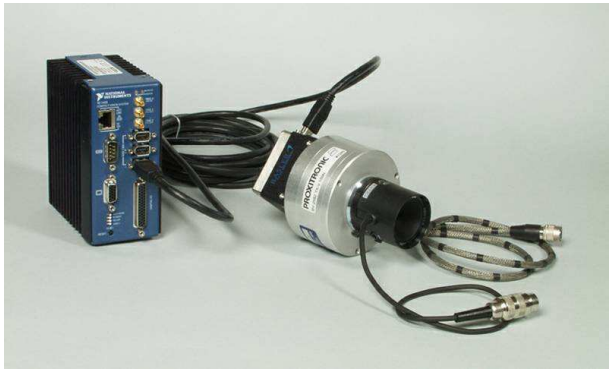

Figure 6: The lens system, image intensifier, digital CCD camera and the CVS front-end digitalization for the BIF Monitor.

Image intensifier: The general scheme of the image intensifier is shown in Fig. 1 and a photo of the realized device in Fig. 6. The light is converted to electrons by a photo-cathode made of S20 UV-enhanced [8], having a quantum-efficiency of $25 - 30\%$ at the requested wavelength interval and a low dark current ($\sim$500 electrons/s$\cdot$cm^2). The voltage between the photo-cathode and the following Multi Channel Plate (MCP) can be switched from a blocking mode for the photo-electrons to a transfer mode within 100 ns enabling an observation exactly during the beam delivery. This drastically reduces the background given by dark counts i.e. spontaneous emission of photons from the photo-cathode or the MCP. In addition, a possible beam width variation within the macro pulse is observable using this fast switching. A two-fold MCP with Ø 25 mm amplifies the photo-electrons with a gain of $\sim 10^6$. On the following P46 fast phosphor screen a spot of each single photo-electron is visible. Due to the phosphor decay time of $\sim$300 ns (90% to 10 %) fast changes of the beam parameters can be resolved. The spatial resolution of $\sim$0.1 mm on the MCP surface is sufficient for our application. This image intensifier was fabricated by the company Proxitronic [8].

Taper coupling: For the light transmission from the Ø 25 mm phosphor to the 1/2"standard Sony CCD chip (6.4×4.8 mm^2) we used a minifying taper coupling made of bundled glass fibers and a minification of 25/8 (ratio of MCP and CCD diameter) for the first tests. For the permanent installation a lower minification by a 25/15 taper was used to enable a larger image and a shorter distance to the beam center. About 10 % of the light emitted in the half hemisphere is guided to the CCD. Compared to relay optics made by a second standard lens combination a factor of $\sim$5 higher light transmission is achieved. The disadvantage of this choice is, that the CCD chip cannot be exchanged easily in case of a damage by the radiation level produced by the beam.

CCD camera: For the first tests, a 8 bit CCD camera Basler A302fs with 782×582 pixels were chosen. For the later installation, we use a 12 bit Basler 311f with VGA 640×480 pixel resolution to achieve higher dynamics. This camera is shown in Fig. 6. The accumulated charges of the pixels are directly digital-converted at the camera head and transferred using Firewire IEEE 1394 protocol. Compared to an analog video link, no degradation of the image quality due to long cable occurs. The Firewire serial bus standard [9] enables a data rate up to 400 Mb/s, corresponding to more than 60 full-frames per second. The possible variable bus architecture with up to 63 nodes is well suited for the distributed diagnostic installations in various transfer-lines. The maximum cable length for electrical transmission is 5 m. Therefore fiber optic extenders are used for the data transfer to the control room.

Data analysis: After decoding the optical signal to electronics signals, the image data can be recorded by a standard Firewire-PCI interface on a Window-PC. The analysis software is written in LabVIEW. It uses the Firewire driver for the commercial package IMAQ to acquire the images and IMAQ Vision for the image processing. At the time being, a professional data acquisition using a **C**ompact **V**ision **S**ystem **CVS** 1456 from National Instruments under RT-LabVIEW is under preparation, thi hardware is shown in Fig. 6. The data display and analysis will be performed under LINUX using Qt-libraries.

EXAMPLE AND BASIC PROPERTIES OF BIF IMAGES

At the GSI LINAC the beam profile should be monitored within a single macro pulse of 100 μs to 5 ms duration. Therefore the use of a long integration to improve the signal-to-noise ratio is impossible. Due to the low amount of emitted photons, a large amplification of 10^6 is required by the double MCP inside the image intensifier. Two typical raw images are displayed in Fig. 7 together with the vertical profile as yielded from the projection along the

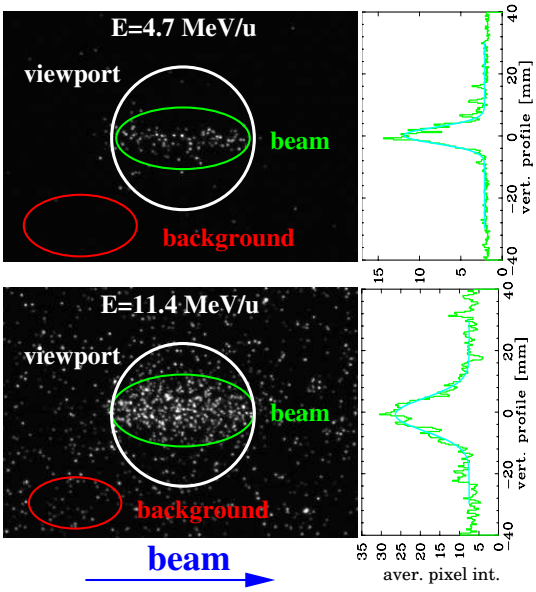

Figure 7: The two dimensional image from the intensifier of a Ar^{10+} beam at 4.7 MeV/u as well as 11.4 MeV/u and $I_{beam} = 2.5$ mA recorded during *one* 250 μs long macro-pulse with a vacuum pressure of about 10^{-5} mbar. The projection for the vertical beam profile (right) are shown [10].

beam path. Each light spots in the raw image is created by one single photon. Due to the statistical nature of the signal generation, the data can be digitally manipulated by data binning, smoothing or by averaging several images, see Fig. 8. The resolution for these examples of about 300 μm/pixel is sufficient for the displayed parameters. A higher resolution can be reached by varying the distance between the beam axis and the camera and by a proper choice of the optics. This flexible adaption for higher resolution is only limited by the required depth of field for an accurate mapping.

By using a regulated gas valve the pressure could be locally (within 1 m) raised up to 10^{-4} mbar. The pressure bump does not show a measurable influence on the

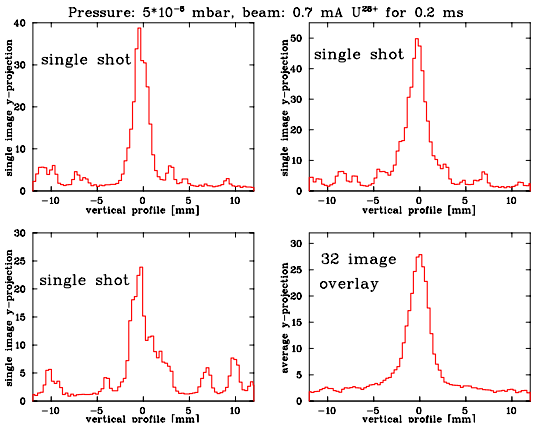

Figure 8: Three vertical projections of images of a single macro pulse and one projection (lower right corner) of an overlay of 32 images. All are made at $5 \cdot 10^{-6}$ mbar [10].

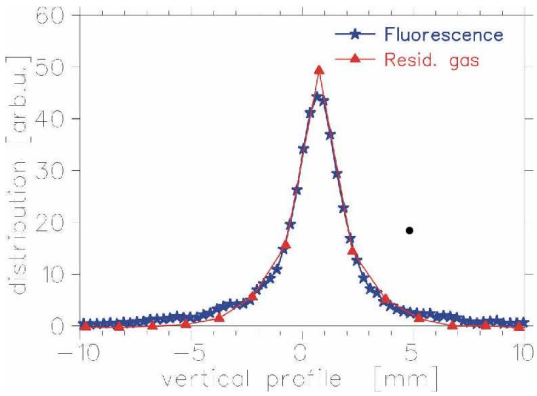

Figure 9: Comparison of the BIF profile with the data of a residual gas monitor. The curves are normalized to the same integral.

ion beam delivered to the GSI synchrotron. For some beam settings a relatively large background was seen, caused by neutrons or γ hitting the photo-cathode. Due to the homogeneous distribution it can easily be subtracted. But a better shielding against neutrons might be desirable for a fail-save application.

Within one order of magnitude, the pressure had been varied and the integrated signal strength shows a linear behavior. The dominant contribution of single step excitations of the mentioned N_2^+ $B^2\Sigma_u^+ \rightarrow X^2\Sigma_g^+$ transitions is verified by that. Behind the synchrotron the pressure could be varied of three orders of magnitude showing also a linear scaling, see below.

The BIF data has been compared with the data of a residual gas monitor located 1m downstream in the beam line. As it can easily be seen in Fig. 9 the correspondence is excellent. This has been verified for many different beam conditions with respect to the measurement with a standard SEM-grid. The resolution of the BIF profile determination can be chosen to be as high as 100 μm/pixel, whereas the SEM-Grid or the residual gas monitor reaches their resolution limit of about 1 mm due to the wire spacing. This is

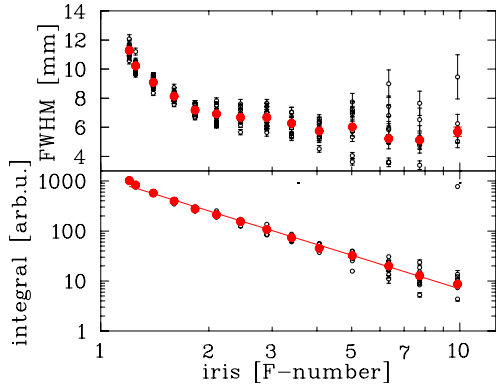

Figure 10: The profile width and the total intensity as a function of the iris setting. The individual images are shown as thin dots and the average of 10 macro-pulse as thick dots [10].

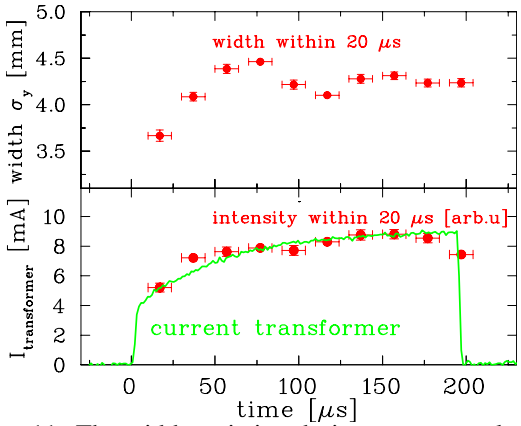

Figure 11: The width variation during a macro-pulse of 8 mA Ar^{10+} at 11 MeV/u is shown. The lower graph compares the normalized image intensity with the beam current [10, 11].

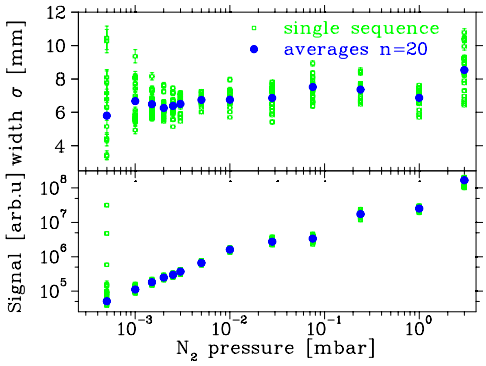

Figure 12: Measured profile width σ and total signal amplitude shown as a function of vacuum pressure. The beam parameter for these measurements were: A 1.5 μs long pulse of $2 \cdot 10^9$ Xe^{48+} ions at 200 MeV/u and a vacuum pressure of $1 \cdot 10^{-3}$ mbar [12].

a massive limitation especially in case of a narrow beam where only a few sample points are distributed over the whole peak, see Fig. 9 as an example.

A crucial point for the operation of the fluorescence monitor is a proper alignment of the optics. In particular the focal distance has to be chosen to coincide with the center of the beam to yield a sufficient large depth of field. As shown in Fig. 10 a sharp image, and therefore a proper width reading, is only created by a partial closed iris. In return fora closed iris the total light intensity is reduced.

APPLICATION: WIDTH VARIATION DURING MACRO PULSES

An advanced application is the determination of a possible and in most cases unwanted variation of the beam profile during the macro pulse, as shown in Fig. 11. Within a rise time of $\tau_{rise} = 100$ ns the voltage between the photocathode and the MCP can be switched from blocking mode to photo-electron transmission toward the MCP. This can be used to restrict the exposure time during the profile measurement. For the case of Fig. 11 one image of 20 μs exposure time is recorded and these short term measurements are repeated with 10 different trigger delays for consecutive macro-pulses. This time-resolved profile determination is not possible with an intercepting SEM-grid due to the risk of wire melting by the large beam power.

SIGNAL DEPENDENCE ON N_2 PRESSURE FOR HIGH BEAM ENERGIES

The method can not only be applied at the GSI LINAC with beam energies up to 15 MeV/u, but also for higher energies as delivered by the GSI synchrotron SIS18. In particular, this is important for the planned FAIR facility. Due to the higher beam energy, a background contribution caused by neutrons is expected to be larger. The amount of particles behind a synchrotron is smaller than at a LINAC; to compensate this, a higher vacuum pressure is required. For sufficient signal strength on a single shot basis, a relatively large pressure bump of typically 10^{-3} mbar was required for the investigated beam currents. These currents are two to three orders of magnitude lower than expected of FAIR. To legitimate the necessary extrapolation for the FAIR design beam currents, the vacuum pressure was varied via a regulated gas-valve by nearly four orders of magnitude to larger pressures. To compensate for the increasing light intensities, the iris opening was reduced and the MCP-gain was lowered; the recorded profiles were then corrected by the resulting factor. Fig. 12 confirms the pressure independence of the measured profile width σ, while the total signal amplitude increases linearly with the N_2 pressure.

For pressures $p > 1$ mbar, the 2-step excitation process with the fluorescence in the near UV via the $C^3\Pi_u \rightarrow B^3\Pi_u + \gamma$ (see Eq. 2) might become more important and a probability scaling $\propto p^2$ is expected. As the mean free path of electrons at 1 mbar is about 1 mm, these electrons may travel a certain distance prior to the molecular excitation. Therefore the beam-profile can be enlarged. If the UV-light from the 2-step process is suppressed with an optical low-pass filter (GG395) in front of the image intensifier, the measured profile-width is reduced. Even at 2 mbar pressure the contribution is low, as a reduction of only 10% was detected for a beam width $\sigma \sim 8$ mm.

For 200 MeV/u Au^{65+} ions we mapped the spectral response for the case of large vacuum pressure using narrow band 10 nm interference filters associated with nitrogen transitions, see Tab.1. It is shown, that the dominant light arises from the ionic N_2^+ $B^2\Sigma_u^+$ state (see Eq. 1) and not from the neutral N_2 $C^2\Pi_u$ state (see Eq. 2). These type of investigation will be expanded for different beam parameters and vacuum pressures.

Since the vacuum pressure affects the occurrence and the mean free path of secondary e^- and the beam's E-field will displace charged particles as e^- and N_2^+, profile distortions might occur. For next experiments main research will be the influence of pressure and beam's charge density on fluorescence spectra and profile distortion.

Table 1: Comparison of relative N_2 and N_2^+ transition intensities: 200 MeV/u Au^{65+}, p =1·10^{-2}mbar (SIS-18, Nov. 2006) ↔ 200 keV protons, p =2,6·10^{-2}mbar [6]. The first number of the filter-type represents the central wavelength λ_0 and the second number the filter width in units of nm.

filter λ_0	molecule	Au^{65+} (2006)	p ([6], 1961)
390FS10	N_2^+ (0-0)	46±6,8%	72%
430FS10	N_2^+ (0-1)	39±5,9%	19%
470FS10	N_2^+ (0-2)	4±0,7%	4%
337FS10	N_2 (0-0)	11±1,6%	≈4%

SIGNAL DEPENDENCE ON ENERGY FOR HIGH BEAM ENERGIES

The BIF method should be applied for ion beam energies from 100 MeV/u up to 10 GeV/u as provided by FAIR. Beam energy dependent investigations were performed for slowly extracted U^{73+} ions with energies between 60 and 750 MeV/u. The uniformly distributed background was subtracted from the integrated signal and the resulting amplitude is plotted in Fig. 13, top. The energy loss in matter is described by the Bethe-Bloch formula and is characterized by a $\sim q^2/E$ dependence. Because the beam pipe at the location of detection is separated from the transport-lines by a 50 μm stainless steel vacuum window, energy loss $E_{in} - E_{out}$ and energy-dependent electron

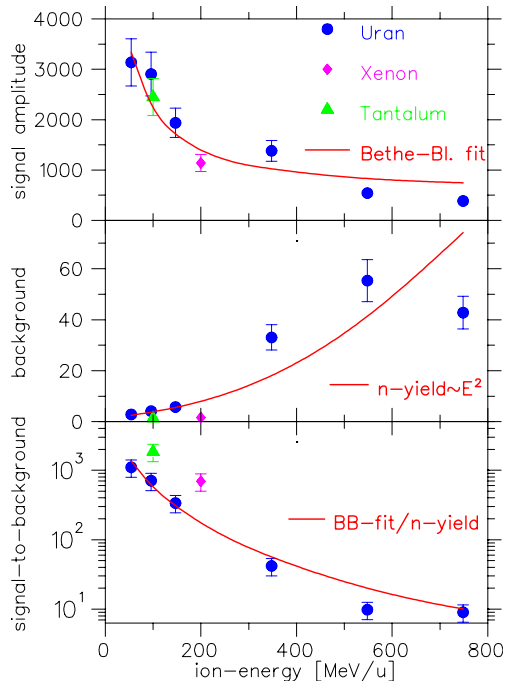

Figure 13: The total signal amplitude (top), background level (middle) and signal-to-background ratio (bottom) as a function of energy for the investigated ions. The signal amplitude for Xe and Ta ere normalized by their charge and mass with respect to U. The background was normalized with respect to the mass only [12].

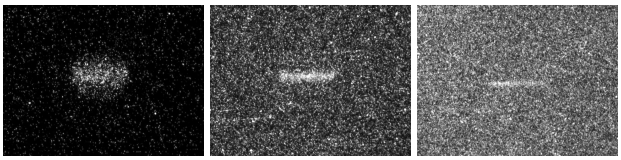

4·10^8U@60MeV/u 1·10^9U@350MeV/u 1·10^9U@750MeV/u

Figure 14: Images from an U beam for different energies and a pressure of $2 \cdot 10^{-3}$ mbar are shown [12].

stripping have to be taken into account. The mean charge states $\overline{q}$ for the accelerated U^{73+} were calculated by the code GLOBAL [13]:

E_{in} [MeV/u]	60	100	150	350	550	750
E_{out} [MeV/u]	52	94	145	346	547	747
Mean charge $\overline{q}$	85.8	88.7	89.7	90.7	90.8	90.9

E_{out} and $\overline{q}^2$ were inserted into the Bethe-Bloch formula and fitted with the parameter a to the fluorescence yield $Y = a\frac{dE}{dx}(E_{out}, \overline{q})$, as shown in relative units in Fig. 13, top. The agreement with the measured signal amplitude is quite good, supporting the proportionality between energy loss and fluorescence yield Y. The data for the other investigated ions Xe and Ta were normalized by the corresponding mass and charge ratios and are described by the same scaling law.

BACKGROUND CONTRIBUTION FOR HIGH BEAM ENERGIES

The most critical issue for the BIF method is the background contribution. As an example, BIF-images for the U beam with three different energies are shown in Fig. 14. The background is uniformly distributed on the image and increases as a function of energy as summarized in Fig. 13, middle. The independence on the iris opening and vacuum pressure judges that the background is not caused by optical photons. Also charged particles can be excluded, due to their limited range in the surrounding material of the image intensifier. In connection with the simulation described below we conclude, that the main source was neutron production in the 2.1 m distant beam-dump. This was also verified by ^{6}Li and ^{7}Li based thermo-luminescence monitors, where ∼80 % of the absorbed dose was due to neutrons. About half of them had energies above 20 MeV.

The cross section of neutron production rises approximately proportional to the square of the energy and to the number of nucleons [14]. These neutrons are scattered and slowed down in the surrounding concrete walls. A realistic model of the beam-dump and the cave walls at ∼ 2 m distance from the beam pipe was used as input for the Monte-Carlo Transport code PHITS [15]. For the case of the 200 MeV/u Xe beam, flux, energy spectrum and time evolution of the neutrons at the BIF Monitor location were simulated. The energy spectrum is consistent with the result of the thermo-luminescence monitor. Due to the scattering in the walls, the neutron arrival at the detector is delayed with respect to their generation. The measured count-rate

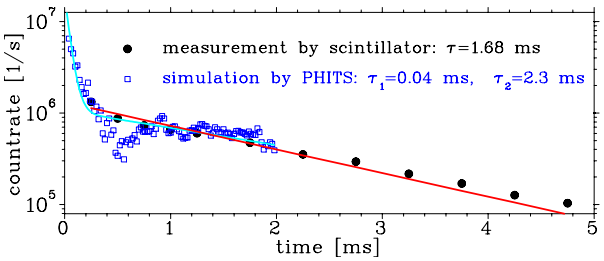

Figure 15: The time evolution of neutron arrival at the BIF Monitor (simulated by PHITS) compared to the counts recorded by a BC400 plastic scintillator. Due to the count rate limitation of the scintillator, the first part up to ~ 0.3 ms is not measured properly [12].

is shown in Fig. 15 and can be approximated by two exponential functions with time constants $\tau_1 = 0.04$ ms and $\tau_2 = 2.3$ ms. It coincides with the measured count rate by a shielded plastic scintillator (decay constant $\tau = 1.7$ ms), which was mainly sensitive to neutrons. The background contribution of the BIF Monitor showed the same time behavior, as determined for the fast extracted Xe and Ta beams of 1.3 μs duration and a varying exposure time of the image intensifier between 3 μs and 15 ms. For the short exposure time matched to the beam delivery, the background contribution was reduced by a factor ~ 4. This is the reason for the improved signal-to-background ratio for the fast extracted Xe and Ta beams in Fig 13, bottom, compared to the slowly extracted U beam. For slow extraction over several seconds, short gating cannot be applied and thus the background contribution is higher.

CONCLUSION

The described non-intercepting BIF method for profile measurements can be applied for ion beams of high current at a pulsed LINAC and extracted beams behind the synchrotron. A modern, cost-efficient and compact design of the monitor hardware was developed and its robust applicability was demonstrated. A direct image of the beam with low background is generated without any installation inside the beam pass. The resolution can easily be adapted to the beam requirements by the flexible optical lens system. A resolution down to 0.1 mm is reachable by large magnification, which is about a factor of 10 better as for a SEM-grid. By extensive beam-based tests it has been shown, that beam profile can well be determined and for the given parameters, no or only low distortions are detectable. The photon yield scales proportional to the electronic stopping power. For higher beam energies a better shielding of the image intensifier against neutrons is required and a design with a fiber-optics bundle is in preparation. For a signal enhancement at lower currents, a moderate pressure bump has to be applied. The BIF method offers advanced detection schemes like observation of a possible beam movement during the macro-pulse by a short exposure time down to several μs due to the switching of the photo cathode voltage. This is not accessible with intercepting methods using SEM-grid. In near future we will investigate even more the properties of the BIF method e.g. by mapping the fluorescence spectrum with the optical filters for various beam and pressure conditions. For very narrow beams, the space charge might influence the trajectory of the ionic N_2^+ molecule prior to the fluorescence emission; this will be investigated experimentally and compared to calculations. Technically we will workout a professional data acquisition and analysis software package to enable the usage of the BIF Monitor as an operating tool.

Acknowledgment: We like to thank W. Barth, L. Groening, D.H.H. Hoffmann and D. Varentsov from GSI for supporting this development and valuable discussions. We acknowledge the support of the European Community-Research Infrastructure Activity under the FP6 "Structuring the European Research Area" programme (CARE, contract number RII3-CT-2003-506395).

REFERENCES

[1] D.P. Sandoval et al., 5^{th} *Beam Instrum. Workshop, Santa Fe, AIP Conf. Proc. 319*, p. 273 (1993).
[2] M.A. Plum et al., *Nucl. Instrum. Meth.* **492**, p. 42 (2002).
[3] G. Burtin et al., *Proc. EPAC 00,* Vienna, p. 256 (2000).
[4] P. Ausset et al., *Proc. EPAC 02,* Paris, p. 1840 (2002).
[5] J. Dietrich et al., *Proc. ICFA-Hadron Beams 2004,* Bensheim p. 184 (2004).
[6] R.H. Hughes et al., *Phys. Rev.* **123**, 2084 (1961).
[7] L.W. Dotchin et al., *J. Chem. Phys.* **59**, 3960 (1973).
[8] www.proxitronic.de.
[9] D. Anderson, *FireWire system architectur: 1394a,* www.mindshare.com, Addison-Wesley (1999).
[10] P. Forck, A. Bank, *Proc. EPAC 02*, Paris, p. 1885 (2002) and A. Bank, P. Forck, *Proc. DIPAC 03*, Mainz, p. 137 (2003).
[11] P. Forck et al., *Proc. DIPAC05*, p. 223, Lyon (2005).
[12] F. Becker et al.,*Proc. EPAC 06*, Edinburgh, p. 1013 (2006).
[13] C. Scheidenberger et al., *Nucl. Instrum. Meth.* **B 142**, 441 (1998).
[14] T. Kurosawa et al., *Phys. Rev.* **C 62**, 044615 (2000).
[15] H. Iwase et al., *JNST*, Vol. 39, No.11, 1142 (2002).